Compact-Size Bandpass Filter for S-Band Transceivers of LEO Satellites

Asmaa E. Farahat and Khalid F. A. Hussein

Microwave Engineering Department
Electronics Research Institute, Cairo, 11843, Egypt
e_asma_e@yahoo.com, Khalid_elgabaly@yahoo.com

Abstract ─ This paper introduces a variety of designs for low-cost and compact-size bandpass filter (BPF) proposed for S-band space-links between ground stations and low earth orbit (LEO) satellites. The proposed designs implement multiple cascaded coplanar waveguide (CPW) resonators with either single or double resonance. The first design is a compact dual-band BPF of dimensions 13×11 mm^2 that can operate simultaneously for both the uplink and downlink in an S-band transceiver. The second design is a single-band BPF of dimensions 25×10 mm^2 that can operate for the space uplink. The third design is a compact single-band BPF of dimensions 17×12 mm^2 that can operate for the space downlink. The three designs are compact size, low cost, and high performance BPFs. The dual-band BPF design is based on dual-resonance mechanism where the resonant structure is constructed as two overlapped quarter-wavelength and half-wavelength CPW resonators; each of them operates in its first-order resonance. The single-band design is based on a quarter-wavelength CPW resonator. Three prototypes are fabricated for the proposed filter designs and their frequency responses are assessed through simulation and experimental measurements showing good agreement. It is shown that the implemented designs satisfy the operational requirements for the assigned space link with high performance, good impedance matching, and low insertion loss.

Index Terms ─ Band-pass filter, CPW resonator, S-band transceiver.

I. INTRODUCTION

S-band communication systems are commonly used in low earth-orbit (LEO) satellites and ground stations for high speed data transfer, for example video or high-quality image data transmission. Usually, an S-band transceiver is used in such type of satellites to provide a high-speed data downlink for payload and low-speed data transfer uplink for telecommand [1], [2]. Due to application requirements, the frequency band for the downlink is much wider and centered at higher frequency than that of the uplink with reasonably wide separation between the two bands. For example, the downlink may be centered at 2250 MHz with bandwidth of 100 MHz, whereas the uplink may be centered at 2050 MHz with a bandwidth of 20 MHz or less. The data rate for the downlink is usually few dozens of Mbps whereas the uplink is few hundreds of Kbps. The data transfer rate and bandwidth are arbitrarily chosen according to the application. In the S-band transmitter of LEO satellites, a BPF is used before the power amplifier to prevent its oscillations and to block the undesired harmonics [1]. In the receiver, to avoid some problems in the frequency mixing stage a BPF is added to eliminate the harmonics and spurious signals or nonlinearities caused by the LNA [2].

Modern S-band communication systems for space links require compact size, high-performance narrow-band bandpass filters (BPF) having low insertion loss, sharp response, and high selectivity together with linear phase or flat group delay in the passband [3]. These filtering features are favorable for the applications that require high spectral efficiency [4-7]. BPF design should also have low radiation loss which can be reduced by using planar resonators of low profile such as the coplanar wave guide (CPW) resonator of narrow slots and narrow central strip. This will enhance the quality factor and reduce the insertion loss [8].

A CPW has the principal advantage that the signal line and the signal grounds are placed on the same substrate surface. This eliminates the need for via holes and, thereby, simplifies the circuit fabrication. Another main advantage of the CPW is that it exhibits lower conductor loss than microstrip lines [9], [10]. CPW parameters are not sensitive to the substrate thickness, and a wide range of impedance is achievable on reasonably thick substrates. Also, circuits can be built using both the odd and the even CPW modes [11]. Moreover, CPWs are open structures, and do not require metallic enclosures [11]. Also, a CPW resonator (CPWR) has its distributed element construction avoiding uncontrolled stray inductances and capacitances, and, thereby, has better microwave properties than a lumped element resonator [12].

Due to their practical importance, microwave and

Submitted On: February 27, 2020
Accepted On: March 26, 2020

millimeter-wave bandpass filter design based on CPWRs has attracted the attention of many research works. In [13], the design of high-quality bandpass filter employing shunt inductively coupled CPW resonators is introduced. In [14], across-coupled CPW structure design is proposed for bandpass filter, which is constructed by cascading several sections of quarter wavelength open-end series stubs. In [15] and [16], compact edge-coupled CPW bandpass filter designs are proposed. In [17], an S-band triangular open loop resonator BPF energized using electromagnetic and edge coupling is presented. In [18], a band pass filter based on folded tri-section stepped impedance resonator (FTSIR) and defected ground structure (DGS) is presented. In [19], a dual-band BPF with several attenuation poles is designed using rectangle structure which exhibits very low insertion loss. In [20], dual-band band-pass filter using tri-section stepped impedance resonators with one stub between parallel coupled lines are employed to realize two pass-bands. In [21], a dual band band-pass filter using multilayer structure is presented.

The end-coupled and edge-coupled CPWR structures are commonly used for microwave and millimeter-wave filter design [8]. In end-coupled resonators, the interchange of energy with the coupling gap may be insufficient, even when very narrow gaps are employed. Due to this reason parallel-coupled CPWRs are used in the present work.

The present work proposes two different solutions for narrow-band BPFs required in the S-band communication system of LEO satellites and ground stations for the space uplink and downlink. The first solution is a dual-band BPF design based on a resonant structure constructed as overlapped half-wavelength and quarter-wavelength CPWRs that can work simultaneously for both the uplink and downlink. The other solution provides two designs for a single-band BPF based on quarter-wavelength CPWR; the first design is for a BPF whose passband centered at the operating frequency of the space-uplink, whereas the other design has its passband centered at the operating frequency of the space-downlink.

II. PROPOSED BAND-PASS FILTER DESIGNS

The most common functions of the BPF in a transceiver are to limit the bandwidth of operation, to remove the oscillations of the amplifier and to reduce the supurious signals and undesired harmonics. Due to size and weight constraints and power limitations, a small satellite transceiver usually implement the sample antenna for simultaneous transmission and reception. Fig. 1 shows the block diagrams for two possible designs of the sattelite S-band tranceiver. Figure 1 (a) shows a tranceiver system that uses one antenna with two separate BPFs. Figure 1 (b) shows a tranceiver system that employs one antenna with dual-band BPF.

The design of higher-order BPF for each pass-band can be based on using cascaded resonators to mediate coupling between the isolated CPW feeding regions as shown in Fig. 2 (a). Each resonator can be either a single-resonance quarter-wavelength CPWR, or a dual-resonance overlapped half-wavelength and quarter-wavelength CPWRs. In Figs. 2 (b) and 2 (c), single-band and dual-band BPFs constructed using one resonator placed between the two feeding CPW regions are shown, respectively. The design of the single-band and dual-band BPFs are discussed in the following two sections.

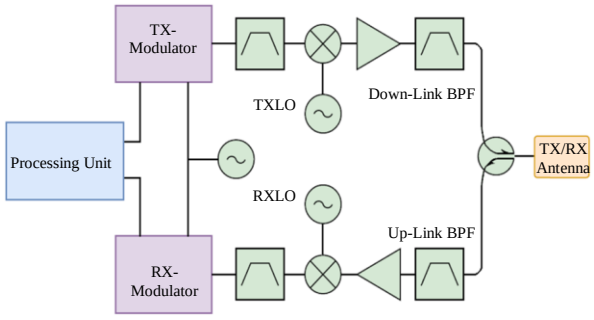

(a) Two separate single-band BPFs

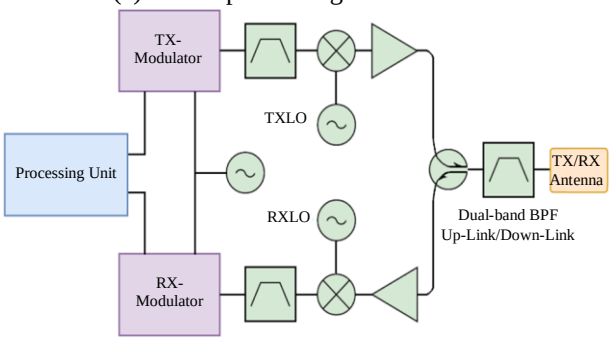

(b) One dual-band BPF

Fig. 1. Block diagrams for two designs of a small satellite S-band transceiver.

According to the above discussion, three designs of a BPF are proposed. The first two designs are single-band BPF, one for the space-uplink, and the other for the space-downlink, whereas the third design is a dual-band BPF that can operate for both uplink and downlink simultaneously.

A. Single-band bandpass filters for uplink and downlink

A single-band BPF with the geometry shown in Fig. 2 (b) is proposed for S-band transmitters and receivers of LEO satellites. This filter is constructed as a symmetric structure composed of two feeding (normally isolated) corner-shaped CPW regions which are (capacitively) parallel-coupled to a quarter-wavelength CPWR of

relatively wide central conductor. This CPWR is open-circuited at the base of the U-shape and short-circuited at the other end (top of the U-shape). As long as the operating frequency is far from the resonant frequencies of the CPWR, the two corner-shaped CPW feeding regions are isolated from each other and no power transfer occurs between the filter ports (1) and (2). Only at the resonant frequencies, the CPW feeders are parallel-coupled to the quarter wavelength CPWR and, hence, the power transfer can occur over narrow bands at these frequencies leading to a narrow-band bandpass filter response.

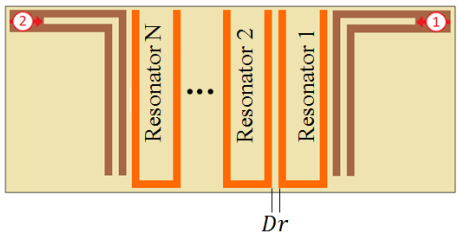

(a) Higher-order BPF based on cascaded CPW resonators

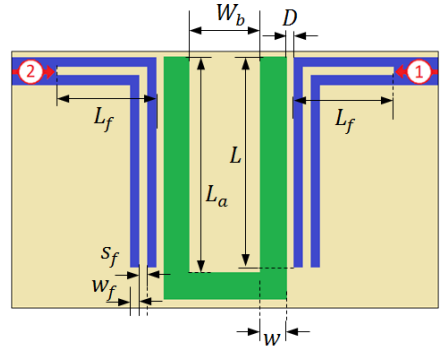

(b) Single-band BPF

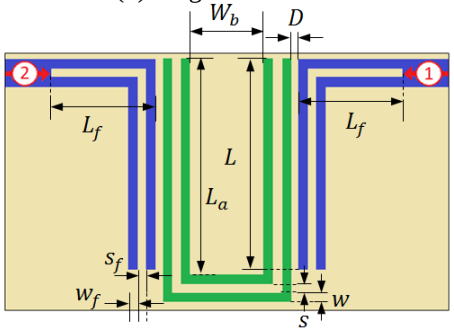

(c) Dual-band BPF

Fig. 2. Proposed designs for the S-band BPF for small satellite transceiver

B. Dual-band bandpass filter

A dual-band BPF with the geometry shown in Fig. 2 (c) is proposed for S-band transceivers of LEO satellites. This filter is constructed as two feeding CPW regions parallel-coupled to the dual-resonant CPW structure which is composed of two overlapped resonators. One of them is a half-wavelength CPWR, which is short-circuited at its both ends and forms the perimeter of U-shape. The other resonator is a straight CPWR of relatively wide central conductor formed by the area subtended between the arms of the U-shape. This CPWR is open-circuited at the base of the U-shape and short-circuited at the other end (top of the U-shape) and, thus forms a quarter-wavelength resonator. As long as the operating frequency is far from the resonant frequencies of the dual CPWR structure, the corner-shaped CPW feeding regions are isolated from each other leading to zero power transfer between the filter ports (1) and (2). Power transfer between the filter ports can occur only at the resonant frequencies, when the CPW feeders are parallel-coupled to the dual-resonant CPW structure. As the resonances of the overlapped half-wavelength and quarter-wavelength resonators are shifted from each other, the structure can be dual-band bandpass filter where the frequency separation between the two bands can be controlled by the filter dimensional parameters.

III. THEORETICAL BASICS

A. Half-wavelength and quarter-wavelength CPW resonators

The resonance frequency for a CPWR can be expressed as [22]:

$$f_n^{(1/2)} = \frac{n\,c}{2L_R\sqrt{\varepsilon_{r_{eff}}}}\ ,\ f_n^{(1/4)} = \frac{(2n-1)\,c}{4L_R\sqrt{\varepsilon_{r_{eff}}}}, \tag{1}$$

where L_R is the total length of the resonator, $f_n^{(1/2)}$ and $f_n^{(1/4)}$ are the resonant frequencies of the half-wavelength resonator and quarter-wavelength resonator, respectively, c is the velocity of light in free space, n is the resonance mode order, $n = 1,2,\ldots$, and $\varepsilon_{r_{eff}}$ is the effective dielectric constant of the quasi-TEM mode of the CPW, and L_R is the length of the resonator.

The effective dielectric constant and the characteristic impedance of the quasi-TEM mode of the CPW can be expressed as [22]:

$$\varepsilon_{r_{eff}} = 1 + \frac{\varepsilon_r - 1}{2}\frac{K(\acute{k}_0)}{K(k_0)}\frac{K(k_1)}{K(\acute{k}_1)},$$
$$Z_0 = \frac{30\pi}{\sqrt{\varepsilon_{r_{eff}}}}\frac{K(\acute{k}_0)}{K(k_0)}, \tag{2}$$

where ε_r is the dielectric constant of the substrate material and K denotes the complete elliptic integral of the first kind, which is defined as:

$$K(k) = \int_0^{\frac{\pi}{2}} \frac{d\theta}{\sqrt{1 - k\sin^2\theta}}. \tag{3}$$

The arguments, k_0, $\acute{k}_0$, k_1, and $\acute{k}_1$, of K are defined as follows:

$$k_0 = \frac{s}{s + 2w}, \tag{4a}$$

$$\acute{k}_0 = \sqrt{1 - k_0^2}, \quad (4b)$$

$$k_1 = \frac{\sinh(\pi s/4h)}{\sinh[\pi(s+2w)/4h]}, \quad (4c)$$

$$\acute{k}_1 = \sqrt{1 - k_1^2}, \quad (4d)$$

where s is the width of the central conductor and w is the width of each side slot.

In spite of being formulated for a CPW of infinitely extending ground, the expressions (2)-(4) can be used as preliminary design rules for a CPW with side ground strips of finite width with good accuracy. According to (2), a 50Ω characteristic impedance of the CPW printed on a substrate of specific material can be obtained by setting the proper values of the strip and slot widths (s, w).

B. Estimation of the quality factor of the bandpass filter

Definitely, the parallel coupling between the resonator and the feeding CPW regions has the effect of external capacitive loading on the resonator. As a consequence, the resonance frequency can be shifted due to such reactive coupling because part of the energy is stored in the electric field of the coupling capacitance. Besides, due to such capacitive coupling, the resultant (loaded) quality factor, Q, is decreased as the coupling to the feeding CPW regions can be considered as a loss channel. The external quality factor Q_e, which is related to the coupling effect as well as the radiation loss dominates the resultant (loaded) quality factor. Thus, the total quality factor can be evaluated through the following relation:

$$\frac{1}{Q} = \frac{1}{Q_u} + \frac{1}{Q_e}, \quad (5)$$

where, Q_u is the self (also, known as internal or unloaded) quality factor of the CPWR. Theoretically, a lossless CPWR has infinite unloaded Q-factor, $Q_u = \infty$. However, practically, Q_u is limited by the conductor and dielectric losses. It should be noted that, for low-loss CPWR, the external Q-factor Q_e, dominates the total Q-factor expressed by (5).

The external Q-factor can be expressed as follows:

$$\frac{1}{Q_e} = \frac{1}{Q_R} + \frac{1}{Q_C}, \quad (6)$$

where Q_R is an equivalent Q-factor related to the radiation loss and Q_C is an equivalent Q-factor related to the reactive coupling between the resonator and feeding CPW regions.

B.1. Calculating the unloaded quality factor of the CPWR

The unloaded Q-factor of both short-circuited and open-circuited half-wavelength CPWR can be expressed as follows [5]:

$$Q_u = \frac{\pi}{2\alpha L_{R_{1/2}}} = \frac{\beta_0}{2\alpha}\sqrt{\varepsilon_{r_{eff}}} = \frac{\omega_0}{2c\alpha}\sqrt{\varepsilon_{r_{eff}}}, \quad (7)$$

where, $L_{R_{1/2}}$ is the length of the half-wavelength resonator, β_0 is the free space wave number, ω_0 is the resonant angular frequency, α is the attenuation constant of the CPW, and $\varepsilon_{r_{eff}}$ is given by (2).

The attenuation constant α of the CPW is related by the conductor and dielectric losses and, hence it can be expressed as follows:

$$\alpha = \alpha_c + \alpha_d, \quad (8)$$

where, α_c is the attenuation caused by the conductor loss whereas α_d is the attenuation caused by the dielectric substrate loss. For a transmission line made of high-conductivity metals like copper ($\sigma = 5.6 \times 10^7 \mathrm{S/m}$) the dielectric loss dominates, which means that $\alpha_d \gg \alpha_c$ and, hence, for a CPW carrying TEM mode, the attenuation constant can be approximated as follows:

$$\alpha \approx \alpha_d = \frac{\omega_0 \tan\delta}{2c}\sqrt{\varepsilon_{r_{eff}}}. \quad (9)$$

Making use of (9), the expression (7) of the unloaded Q-factor of the CPWR reduces to the following:

$$Q_u \approx \frac{1}{\tan\delta}. \quad (10)$$

Substituting from (10) into (5), the total quality factor can be expressed as

$$Q \approx \frac{Q_e}{1 + Q_e \tan\delta}. \quad (11)$$

The last expression can be used to calculate the external Q-factor, Q_e, if the loss tangent of the dielectric substrate is known given that Q has been obtained by simulation.

IV. RESULTS AND DISCUSSIONS

In the present section, both the numerical results obtained by microwave simulation using CST® software package and the experimental results obtained by microwave measurements of some fabricated S-band BPF prototypes are presented, discussed and compared for the purpose of arriving at accurate performance assessment of the proposed filter designs. The first solution proposes a dual-band BPF for both the high-speed payload data downlink and the low-speed telecommand data uplink. The second solution proposes two designs for single-band BPF one for the uplink and the other for the downlink.

A. Comparative performance of multi-resonator BPF

This section is concerned with the performance assessment of a single-band BPF employing single, double, and triple quarter-wavelength resonators arranged as shown in Fig. 2 (a). The design dimensions are $w = 0.4$ mm, $L_a = 15.3$ mm, $L = 14$ mm, $L_f = 4.4$ mm,

$s_f = 0.5$ mm, $w_f = 0.4$ mm, $W_b = 1$mm, $D = 0.2$ mm, and $Dr = 0.1$mm. The frequency responses of the transmission coefficients for three single-band resonators BPF centered at 2.02 GHz are plotted in Fig. 3.

As shown in Fig. 3, it is clear that with increasing the number of cascaded resonators (of the same dimensions), the resulting filter have larger size, wider bandwidth, sharper response and higher rejection ratio in the stop bands. In all the cases, the insertion loss seems to be the same which is low enough to be acceptable for the three designs. However, as it is preferable to have a BPF with compact size and narrow bandwidth for small satellite transceivers as discussed earlier, a single-resonator can be used to implement the required S-band bandpass filter for both single-band and dual-band operations.

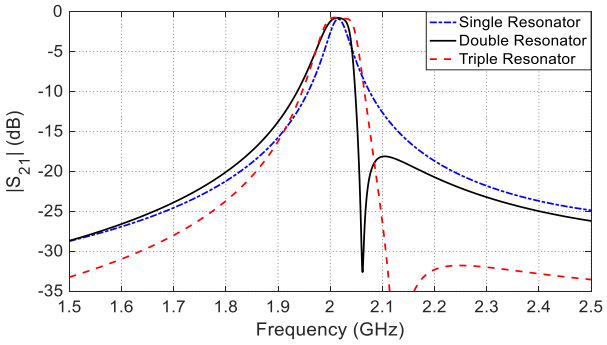

Fig. 3. Frequency response of the transmission coefficient $|S_{21}|$ for single-band BPF designs employing one, two, and three resonators.

B. Dual bandpass filter for S-band transceiver of small satellites

The following presentations and discussions of numerical and experimental results are concerned with a dual-band BPF for S-band transceiver of small LEO satellites as that shown in Fig. 2 (c) designed with the following dimensional parameters, unless otherwise stated. $s = 0.3$ mm, $s_f = 1.1$ mm $w = w_f = 0.4$ mm, $W_b = 2.6$ mm, $L_a = 12.8$ mm, $L_f = 5$ mm, $D = 0.35$ mm, and $L = 12.7$ mm. The substrate material is Rogers RO3010™ with dielectric constant $\varepsilon_r = 10.2$, and height $H = 1.27$ mm. The metal strips and ground are made of copper and have conductivity $\sigma = 5.6 \times 10^7 S/m$.

The frequency response of the transmission coefficient, $|S_{21}|$ and reflection coefficient, $|S_{11}|$ of the proposed dual-band BPF is shown in Fig. 4. The $|S_{21}|$ curve exhibits two peaks. the first peak is at $f = 2.08$ GHz, with frequency bandwidth of 80 MHz, whereas the second peak is at $f = 2.3$ GHz, with frequency bandwidth of 60 MHz. The mechanisms of resonance leading to these values of the resonant frequencies and the corresponding quality factors are explained in the following subsection.

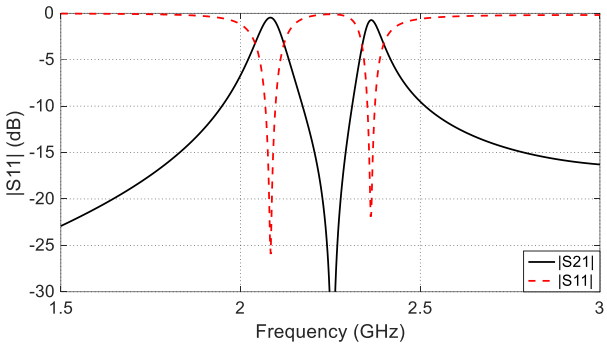

Fig. 4. frequency response of the transmission and reflection coefficients $|S_{21}|$ and $|S_{11}|$ of dual-band BPF designed for S-band tansceiver of a LEO satellite; the lower frequency pass band is for the uplink and the higher frequency pass band is for the downlink.

B.1. Mechanisms of resonance for dual-band operation

The two corner-shaped CPW regions of the main feeder are coupled to each other only at the resonances of each of the two CPWRs formed by the U-shape as mentioned in Section II.B. The frequency response of the filter transfer function has two peaks as shown in Fig. 4. The first peak corresponds to the first resonance of the half-wavelength CPWR on the perimeter of the U-shape which is short-circuit terminated at its both ends. The second peak corresponds to the first resonance of the quarter-wavelength CPWR whose central conductor is the area subtended between the arms of the U-shape. The side (ground) conductors for this CPW are actually the central conductor of the CPW on the perimeter of the U-shape mentioned in section II.B. As shown in Fig. 2 (c), these side conductors have much narrower width in comparison to the width of the central conductor. This resonator is open-ended at the base of the U-shape and is short-circuit terminated at the other end. This is more elaborated showing illustrations of the current and field distributions on the resonator in the following two subsections.

B.1.1. Mechanism of resonance in the lower frequency band

At the lower resonant frequency (2.08 GHz) of the short-ended CPWR formed by the perimeter of the U-shape, the surface current distribution is presented in Fig. 5 (a). It is shown that, like a short-ended half-wavelength resonator, the current has its maximum magnitude at the short-circuited terminals of the resonator whereas the current node of the standing wave is at the middle of the resonator length. The electric field distribution in the slots of this CPW is presented in the same figure which exhibits the behavior of the (even) quasi-TEM mode of the CPW formed by the arms of the U-shape. As this CPWR is half-wavelength whose length is 30.25 mm,

the resonant frequency can be calculated using (1-a), which gives $f_1^{(1/2)} = 2.12$ GHz. The slight deviation of the resonant frequency obtained by simulation from the theoretical value can be attributed to the error due to approximate analytical formula for $\varepsilon_{r_{eff}}$ given by (2) and due to the reactive load caused by coupling to the CPW feeder regions which leads to a shift of the resonant frequency.

B.1.2. Mechanism of resonance in the higher frequency band

At the higher resonant frequency (2.3 GHz) of the quarter-wavelength CPWR whose central conductor is the region subtended between the arms of the U-shape, the surface current distribution is presented in Fig. 5 (b). This CPW region is open-ended at the base of the U-shape and is short-ended at its other end. It is shown that, like a quarter-wavelength resonator, the current has its maximum magnitude at the short-circuit terminal whereas the current node is at its open-ended. The length of this CPWR is 12.8 mm, and hence, the resonant frequency can be calculated using (1-b), which gives $f_0^{(1/4)} = 2.311$ GHz. The slight deviation of the resonant frequency obtained by simulation from the theoretical value can be attributed to the error of the approximate analytical formula given by (2) for $\varepsilon_{r_{eff}}$ and to the reactive load caused by capacitive coupling of the CPW feeder regions which, in turn, leads to a shift of the resonant frequency.

B.2. Experimental assessment of dual-band BPF proposed for S-band transceiver

A prototype of the proposed dual-band BPF is fabricated for experimental investigation of the filter performance. The substrate used for fabrication is Rogers RO3010™, with substrate height h = 1.27 mm, dielectric constant $\varepsilon_r = 10.2$ and dielectric loss tangent $\delta = 0.0021$. The same design dimensions given at the beginning of Section IV.B are used for fabrication. A photograph of the fabricated prototype is presented in Fig. 6 whose size is compared to a coin of the standard one-inch diameter size.

The vector network analyzer (VNA) of Keysight (Agilent) FieldFox N9918A™ is used to measure the transmission and reflection coefficients $|S_{21}|$ and $|S_{11}|$, respectively, of the dual-band BPF prototype under test. For this purpose, the filter prototype is mounted on the substrate test fixture as shown in Fig. 7 (a). After performing the required settings and calibration procedure, the test fixture holding the prototype under test is connected to the VNA as shown in Fig. 7 (b).

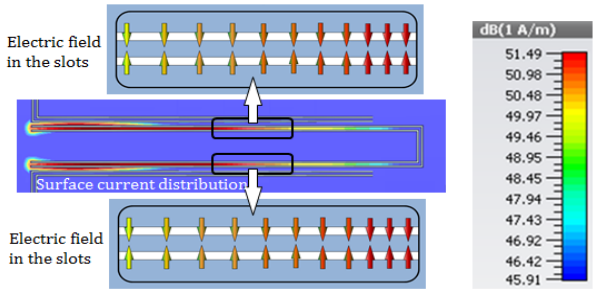

(a) Short-ended half-wavelength CPWR at f = 2.08 GHz

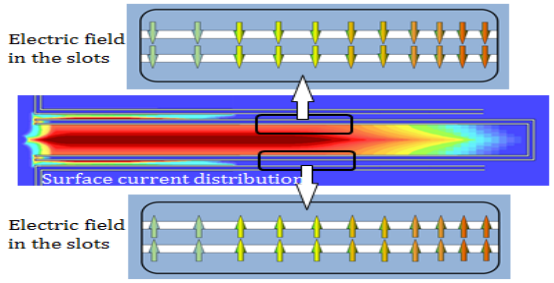

(b) Open-ended quarter-wavelength CPW resonator, f = 2.3 GHz

Fig. 5. Surface current on the conductors and electric field in the slots at the resonant frequency

Fig. 6. Photograph of the fabricated prototype of the dual-band BPF proposed for S-band transceivers of LEO satellites.

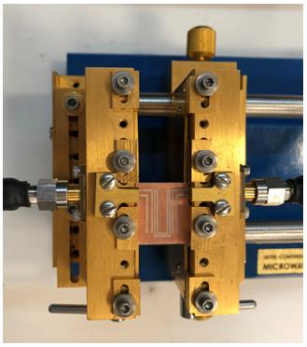

(a) The fabricated BPF mounted on the VNA test fixture

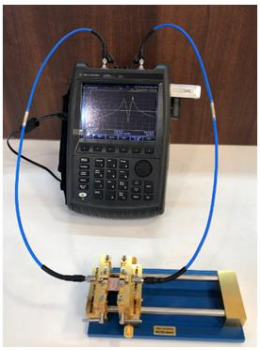

(b) Measurement of the transmission coefficient $|S_{21}|$ using the VNA

Fig. 7. Measurement of the frequency response of the fabricated prototypes for experimental investigation of the proposed BPF.

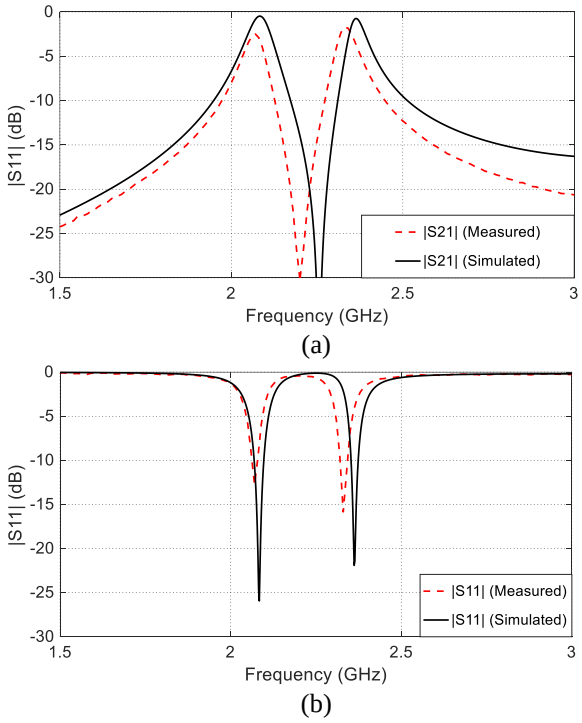

Fig. 8. (a) Frequency response of the transmission coefficient $|S_{21}|$ of the dual-band BPF proposed for S-band transceivers of LEO satellites. (b) Frequency response of the reflection coefficient $|S_{11}|$ of the proposed dual-band BPF for S-band transceivers of LEO satellites.

The frequency response of the transmission coefficient $|S_{21}|$ of the fabricated prototype for the BPF employing half-wavelength CPWR subtending a quarter-wavelength CPWR as measured by the VNA Keysight FieldFox N9918A is presented in Fig. 8 (a) and compared to that obtained by simulation using the CST® software package. Both the experimental and simulation results show good agreement except for a little shift of the resonant frequency, which is, most probably, attributed to the losses encountered in the measurement process. The frequency response of the reflection coefficient $|S_{11}|$ is shown in Fig. 8 (b). The dimensions of the fabricated dual-band BPF are 13×11 mm^2 and hence, it provides a very practical compact and low cost solution for S-band transceivers.

C. Single-band BPF for S-band transceivers of small satellites

Two single-band BPFs having the same design as that shown in Fig. 2 (b), are fabricated with the dimensional parameters listed in Table 1. The single-band BPFs are proposed for S-band transceiver uplink and downlink. The uplink S-band BPF is designed on Rogers RO5880™, with substrate height $h = 1.57$ mm, dielectric constant $\varepsilon_r = 2.2$ and dielectric loss tangent $\delta = 0.0009$. The downlink is designed on Rogers RO3010™, with substrate height $h = 1.27$ mm, dielectric constant $\varepsilon_r = 10.2$ and dielectric loss tangent $\delta = 0.0021$.

Table 1: Design parameters of the proposed single-band BPFs for the S-Band LEO satellite transceiver of small satellites

Dimensional Parameter	Downlink BPF	Uplink BPF
s_f	0.5 mm	1.5 mm
w_f	0.4 mm	0.4 mm
W_b	1.1 mm	1.1 mm
L_a	15 mm	28 mm
L_f	4.05 mm	5.95 mm
D	0.4 mm	0.5 mm
L	13.35 mm	28.3 mm
w	0.4 mm	0.4 mm

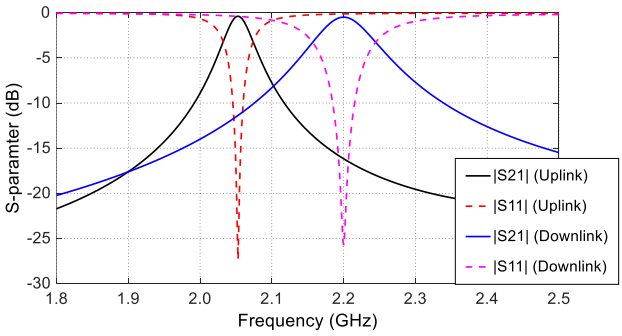

Fig. 9. Frequency responses of the transmission and reflection coefficients of the BPFs proposed for the uplink and the downlink of small satellites S-band transceivers.

The metal strips and ground are made of copper and have conductivity $\sigma = 5.6 \times 10^7 \mathrm{S/m}$ and metal thickness 0.032 mm. The frequency response of the transmission

coefficients $|S_{21}|$ and the reflection coefficient $|S_{11}|$ of the two BPFs are shown in Fig. 9. The uplink BPF has a center frequency of 2.05 GHz and bandwidth of 43 MHz and the downlink BPF has a 92 MHz bandwidth centered at 2.2 GHz.

C.1. Experimental assessment of the proposed single-band BPFs

The prototype of the proposed two single band BPFs are fabricated for experimental verifications. The substrate used for fabrication of the single band BPF used in the uplink is Rogers RO5880™, with substrate height $h = 1.57$ mm, dielectric constant $\varepsilon_r = 2.2$ and dielectric loss tangent $\delta = 0.0009$. The substrate used for fabrication of the single band BPF designed for the downlink is rogers RO3010™, with substrate height $h = 1.27$ mm, dielectric constant $\varepsilon_r = 10.2$ and dielectric loss tangent $\delta = 0.0021$. The same design dimensions given in table 1 are used in the fabrication process. Photographs of the fabricated prototypes are presented in Fig. 10. The experimental setup is the same as that shown in Fig. 7.

The frequency responses of the transmission and reflection coefficients of the BPF shown in Fig. 10 (a) proposed for the S-band space-uplink are measured by the VNA Keysight FieldFox N9918A and presented in Fig. 11 and compared to those obtained by simulation using the CST® software package. Both the experimental and simulation results show good agreement. The slight differences between the measured and simulated results may be due to losses encountered in the measurement process.

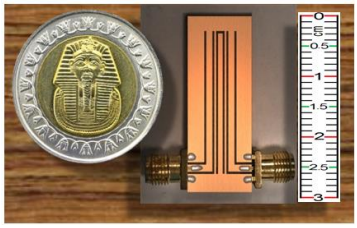

(a) S-band BPF for the uplink

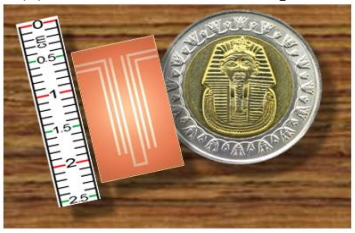

(b) S-band BPF for the downlink

Fig. 10. Fabricated prototype for the proposed single band BPFs used for S-band transceiver.

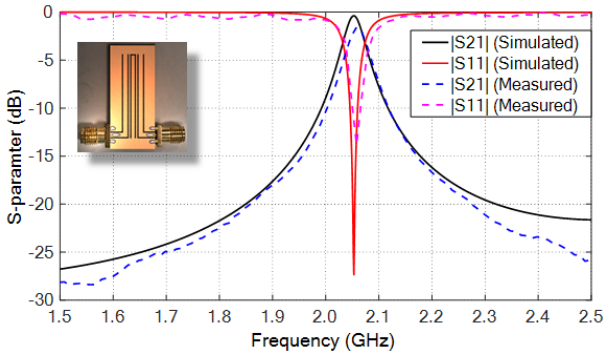

Fig. 11. Frequency responses of the transmission and reflection coefficients $|S_{21}|$ and $|S_{11}|$, for BPF used in the S-band uplink and constructed as two isolated corner-shaped CPW regions partially parallel-coupled to a quarter-wavelength CPWR.

The frequency responses of the transmission and reflection coefficients of the BPF shown in Fig. 10 (b) proposed for the S-band space-downlink are presented in Fig. 12. The center frequency and bandwidth of the proposed single-band BPF can be easily controlled by setting the dimensions of the quarter-wavelength CPWR.

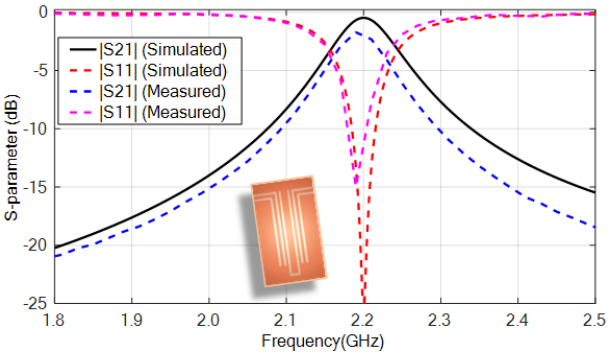

Fig. 12. Frequency responses of the transmission and reflection coefficients $|S_{21}|$ and $|S_{11}|$, respectively, a BPF used in the downlink of S-band tranceiver with the dimensions given in Table 1.

A comparison of the proposed BPF with BPFs found in literature is presented in Table 2.

Table 2: Comparison with similar works

	Size ($\lambda_g \times \lambda_g$)	S_{21}(dB)	S_{11}(dB)
Proposed BPF	0.3 × 0.21	0.63	-27
[17]	0.25 × 0.25	1.3	-25
[23]	0.5 × 0.5	0.1	-25
[24]	0.75 × 0.6	0.04	-23

V. CONCLUSIONS

In this work three compact size, simple structure, low cost, and high performance bandpass filter (BPF) designs for S-band transceiver of LEO satellites are introduced. The first design is a dual-band BPF based on dual-resonance mechanism that can be employed for both the uplink and downlink of the S-band transceiver. The other two designs are based on quarter wavelength CPW resonator. Three prototypes of the proposed filter designs are fabricated and the frequency responses are measured. The experimental measurements show that the implemented designs have high performance with good impedance matching and low insertion loss. The proposed designs are designed on a single layer of the substrate which reduces the substrate losses effect and enhance the quality and performance of the BPF.

The single-band BPF filter is easily controlled as it relies on a single CPWR, its center frequency and quality factor can be accurately tuned. On the other side, the dual band filter is harder to design as the two resonators are overlapped, so it is not easy to tune the center frequency and quality factor for each passband. Employing the dual band BPF or two single band BPFs in an S-band transceiver depends on the transceiver design as mentioned in section 2.

REFERENCES

[1] O. Ceylan, Y. Kurt, F. A. Tunc, H. B. Yagci, and A. R. Aslan, "Low cost S-band communication system design for NANO satellites," *Proceedings of 5th International Conference on Recent Advances in Space Technologies (RAST)*, 2011.

[2] L. Hadj Abderrahmane, M. Benyettou, M. Sweeting, J. R. Cooksley, and P. Garner, "Designing an S-band receiver for LEO applications," *Proceedings of the 11th WSEAS International Conference on Communications*, 26-28, 2007.

[3] J.-S. Hong and M. J. Lancaster, "Couplings of microstrip square open-loop resonators for cross-coupled planar microwave filters," *IEEE Transactions on Microwave Theory and Techniques*, vol. 44, no. 12, Dec. 1996.

[4] J. S. Hong and M. J. Lancaster, *Microstrip Filters for RF/Microwave Applications*. Wiley, New York, 2001.

[5] D. M. Pozar, *Microwave Engineering*. JohnWiley & Sons, Inc., 2012.

[6] F. Vacondio, A. Ghazisaedi, A. Bononi, and L. A. Rusch, "DQPSK. When is a narrow filter receiver good enough," *IEEE Journal of Lightwave Technology*, vol. 27, no. 22, pp. 5106-5114, Nov. 2009.

[7] N. A. Wahab, N. Hidayat, Z. Ismail Khan, Z. Mat Yassin, N. A. Salim, N. Othman, and M. K. M. Salleh, "Two parallel-coupled rings for narrow bandpass filter application," *Journal of Telecommunication, Electronic and Computer Engineering*, vol. 8, no. 373, 2017.

[8] M. Kumar and R. Gowri, "Review on various issues and design topologies of edge coupled coplanar waveguide filters," *Journal of Graphic Era University*, vol. 5, no. 2, pp. 91-96, Jan. 2017.

[9] K. C. Gupta, R. Garg, and I. Bahl, *Microstrip Lines and Slotlines*. Dedham, MA Artech, 1979.

[10] A. Gopinath, "Losses in coplanar waveguides," *IEEE Transactions on Microwave Theory and Techniques*, vol. 30, no. 7, pp. 1101-1104, 1982.

[11] A. V. Sakthivel, A. Sunil, and N. Archak, "Design and implementation of a bandpass coplanar waveguide filter," *Technical Report*, Mar. 2017.

[12] M. Göppl, A. Fragner, M. Baur, R. Bianchetti, S. Filipp, J. M. Fink, P. J. Leek, G. Puebla, L. Steffen, and A. Wallraff, "Coplanar waveguide resonators for circuit quantum electrodynamics," *Journal of Applied Physics*, vol. 104, no. 11, p. 113904, 2008.

[13] J. K. A. Everard and K. K. M. Cheng, "High performance direct coupled bandpass filters on coplanar waveguide," *IEEE Transactions on Microwave Theory and Techniques*, vol. 41, no. 9, pp. 1568-1573, 1993.

[14] R. El Haffar, A. Farkhsi, O. Mahboub, and N. A. Touhami, "Compact size coplanar waveguide bandpass filter design and modeling," *Proceedings of the 2nd International Con.3ference on Computing and Wireless Communication Systems*, (p. 49) ACM, Nov. 2017.

[15] J.-M. Yan, L. Cao, and H.-Y. Zhou, "A novel quad-band bandstop filter based on coupled-line and shorted stub-loaded half-wavelength microstrip resonator," *Progress In Electromagnetics Research*, 65-70, 79, 2018.

[16] O. A. Safia, A. A. Omar, and M. C. Scardelletti, "Design of dual-band bandstop coplanar waveguide filter using uniplanar series-connected resonators," *Progress In Electromagnetics Research*, vol. 27, pp. 93-99, 2011.

[17] B. George, N. S. Bhuvana, and S. K. Menon, "Compact band pass filter using triangular open loop resonator," *Progress In Electromagnetics Research Symposium*, Nov.19-22, 2017.

[18] N. M. Garmjani and N. Komjani, "Improved microstrip olded tri-Section stepped impedance resonator bandpass filter using defected ground structure," *Applied Computational Electromagnetics Society (ACES) Journal*, vol. 25, no. 11, Nov. 2010.

[19] L. P. Zhao, X. Zhai, B. Wu, T. Su, W. Xue, and C.-H. Liang, "Novel design of dual-mode bandpass filter using rectangle structure," *Progress In Electromagnetics Research B*, vol. 3, pp. 131-141, 2008.

[20] D. C. Ma, Z. Y. Xiao, L. L. Xiang, X. H. Wu, C. Y.

Huang, and X. Kou, "Compact dual-band bandpass filter using folded SIR with two stubs for WLAN," *Progress In Electromagnetics Research*, vol. 117, pp. 357-364, 2011.

[21] S. Majidifar and S.-V. Makki, "Dual band bandpass filter using multilayer structure," *Applied Computational Electromagnetics Society (ACES) Journal*, vol. 30, no. 10, Oct. 2015.

[22] R. N. Simons, "Coplanar waveguide circuits, components, and systems," vol. 165, John Wiley & Sons, 2004.

[23] M. S. S. Subramanian, et al., "Design of dual log-spiral metamaterial resonator for X-band applications," *2012 International Conference on Computing, Communication and Applications (ICCCA)*, 2012.

[24] A. Boutejdar, A. Darwish, and A. Omar, "Design and improvement of compact half-wavelength band pass filter employing overlapped slotted ground structure (SGS) and multilayer technique," *Applied Computational Electromagnetics Society (ACES) Journal*, vol. 28, no. 8, Aug. 2013.